



HAL
open science

Biocompatible photoresistant far-red emitting, fluorescent polymer probes, with near-infrared two-photon absorption, for living cell and zebrafish embryo imaging

Salim Adjili, Arnaud Favier, Guillaume Fargier, Audrey Thomas, Julien Massin, Karine Monier, Cyril Favard, Christophe Vanbelle, Sylvia Bruneau, Nadine Peyri eras, et al.

► To cite this version:

Salim Adjili, Arnaud Favier, Guillaume Fargier, Audrey Thomas, Julien Massin, et al.. Biocompatible photoresistant far-red emitting, fluorescent polymer probes, with near-infrared two-photon absorption, for living cell and zebrafish embryo imaging. *Biomaterials*, 2015, 46, pp.70-81. 10.1016/j.biomaterials.2014.12.026 . hal-01142603

HAL Id: hal-01142603

<https://hal.science/hal-01142603>

Submitted on 28 Apr 2022

HAL is a multi-disciplinary open access archive for the deposit and dissemination of scientific research documents, whether they are published or not. The documents may come from teaching and research institutions in France or abroad, or from public or private research centers.

L'archive ouverte pluridisciplinaire **HAL**, est destin e au d p t et   la diffusion de documents scientifiques de niveau recherche, publi s ou non,  manant des  tablissements d'enseignement et de recherche fran ais ou  trangers, des laboratoires publics ou priv s.



Distributed under a Creative Commons Attribution - NonCommercial 4.0 International License

Biocompatible photoresistant far-red emitting, fluorescent polymer probes, with near-infrared two-photon absorption, for living cell and zebrafish embryo imaging

Salim Adjili^{a, b}, Arnaud Favier^{a, b, *}, Guillaume Fargier^c, Audrey Thomas^c, Julien Massin^d,
Karine Monier^a, Cyril Favard^e, Christophe Vanbelle^f, Sylvia Bruneau^{g, h},
Nadine Peyri ras^h, Chantal Andraud^d, Delphine Muriaux^{c, e, **},
Marie-Th r se Charreyre^{a, b, *}

^a Ecole Normale Sup rieure de Lyon, Laboratoire Joliot-Curie, CNRS USR3010, F-69364 Lyon, France

^b INSA-Lyon, Laboratoire Ing nierie des Mat riaux Polym res, CNRS UMR5223, Universit  Claude Bernard Lyon 1, F-69621 Villeurbanne, France

^c Ecole Normale Sup rieure de Lyon, Unit  de Virologie Humaine, INSERM U758, Universit  Claude Bernard Lyon 1, F-69364 Lyon, France

^d Ecole Normale Sup rieure de Lyon, Laboratoire de Chimie, CNRS UMR5182, Universit  Claude Bernard Lyon 1, Site Monod, 46 all e d'Italie, F-69364 Lyon, France

^e Centre d' tudes d'agents Pathog nes et Biotechnologies pour la Sant , CNRS UMR5236, F-34293 Montpellier, France

^f SFR Sant  Lyon Est-CIQLE, CNRS UMS3453/INSERM U57, Universit  Claude Bernard Lyon1, F-69372 Lyon, France

^g UMS AMAGEN, CNRS UMS3504/INRA UMS1374, Bat 32, Avenue de la Terrasse, F-91198 Gif-sur-Yvette, France

^h BioEmergences, CNRS UPS3674, Bat 32, Avenue de la Terrasse, F-91198 Gif-sur-Yvette, France

Exogenous probes with far-red or near-infrared (NIR) two-photon absorption and fluorescence emission are highly desirable for deep tissue imaging while limiting autofluorescence. However, molecular probes exhibiting such properties are often hydrophobic. As an attractive alternative, we synthesized water-soluble polymer probes carrying multiple far-red fluorophores and demonstrated here their potential for live cell and zebrafish embryo imaging. First, at concentrations up to 10 μM , these polymer probes were not cytotoxic. They could efficiently label *living* HeLa cells, T lymphocytes and neurons at an optimal concentration of 0.5 μM . Moreover, they exhibited a high resistance to photobleaching in usual micro-scopy conditions. In addition, these polymer probes could be successfully used for *in toto* labeling and *in vivo* two-photon microscopy imaging of developing zebrafish embryos, with remarkable properties in terms of biocompatibility, internalization, diffusion, stability and wavelength emission range. The near-infrared two-photon absorption peak at 910 nm is particularly interesting since it does not excite the zebrafish endogenous fluorescence and is likely to enable long-term time-lapse imaging with limited photodamage.

1. Introduction

In the last ten years, the number of commercially available exogenous probes dedicated to fluorescence bio-imaging has

known an exponential increase. The most important criteria required by the biologist for the choice of a probe are the biocompatibility, the brightness and the photostability [1]. Other relevant characteristics for bio-imaging are the absorption and emission wavelengths. In fact, probes emitting in the far-red (650–750 nm) and near-infrared (750–950 nm) wavelength range are highly desirable for numerous reasons [2]. First, light absorption/scattering by cells and tissues is very low between 650 and 950 nm, that is called the biological optical window. Second, cell autofluorescence is mainly occurring in the UV and visible wavelength range, although for some cells like human osteoblasts

* Corresponding authors.  cole Normale Sup rieure de Lyon, Laboratoire Joliot-Curie, CNRS USR3010, F-69364 Lyon, France. Tel.: +33 (0)4 72 72 89 38.

** Corresponding author.  cole Normale Sup rieure de Lyon, Unit  de Virologie Humaine, INSERM U758, Universit  Claude Bernard Lyon 1, F-69364 Lyon, France.

E-mail addresses: arnaud.favier@ens-lyon.fr (A. Favier), delphine.muriaux@cpbs.cnrs.fr (D. Muriaux), marie-therese.charreyre@ens-lyon.fr (M.-T. Charreyre).

and hepatocytes, plant cells or zebrafish embryonic cells, autofluorescence can be detected up to 700 nm, which complicates the optical observations [3]. If, in addition, the probe exhibits high two-photon absorption (TPA) efficiency in the near-infrared range, investigation of cells and cellular functions in deep tissue sections and organs can be achieved by two-photon microscopy (TPM). Moreover, TPM can be used for long-term live cell and deep tissue microscopy imaging with reduced phototoxicity and photobleaching since two-photon excitation is spatially localized [4].

One strategy to get exogenous probes with improved brightness and photostability, consists in using fluorescent *polymer* probes instead of *molecular* ones. Generally, this can be achieved by encapsulating numerous molecular dyes inside biocompatible polymer nanoparticles [5]. It can also be achieved by using intrinsically fluorescent π -conjugated polymers [6], encapsulated inside nanoparticles [7] or formulated as polymer dots (Pdots) which have a much smaller size (5–25 nm) than nanoparticles [8]. An alternative strategy to get fluorescent polymer probes of small size consists in covalently binding dyes along a biocompatible polymer chain [9,10]. However, whatever the chosen synthetic route, very few polymer probes emit in the far-red range.

Recently, some polymer dots have been synthesized from donor-acceptor polymer blends to reach visible absorption range and far-red emission and have been used for *in vivo* tumor imaging [11]. Using the dye-polymer binding strategy, Lucas et al. [12] prepared polylysine (PLL) or poly(dimethylaminoethyl methacrylate) (PDMAEMA) based polymers labeled with Cy5 dye ($\lambda_{\text{max Emission}} = 660 \text{ nm}$). These fluorescent cationic polymers were used to complex oligonucleotides and to follow the intracellular dissociation of the polyplexes by confocal imaging. Saad et al. [13] carried out the binding of Cy5.5 dye ($\lambda_{\text{max Emission}} = 710 \text{ nm}$) on the functional groups of a PAMAM dendrimer, further used as nanocarrier for *in vivo* drug delivery. However, in these examples, the polymer structure and/or the dye binding were not controlled and none of those polymer probes were used for two-photon imaging.

In a recent article [14], we reported the design and synthesis of well-defined dye-polymer conjugates, with control over both the polymer chain structure (controlled size, low polydispersity, controlled composition and microstructure) and the dye binding (controlled number of dyes per chain). The remarkable structural homogeneity of these polymer probes was expected to lead to very reproducible bio-labeling results. The chosen dye [15] was emitting in the far-red range, possessed a large Stokes shift and, in addition, was expected to be efficiently excited in the two-photon mode. However, as most of the probes that exhibit interesting TPA properties, it was a hydrophobic fluorophore. Our recent experience with hydrophobic TPA dyes (emitting in the visible range) demonstrated that it is indeed possible to get water-soluble and biocompatible dye-polymer conjugates provided that a biocompatible polymer backbone is used and that the number of dyes per chain is controlled [16]. By tuning the nature of the groups along the polymer chain and the number of far-red dyes per chain, we could synthesize fluorescent polymer probes that were water-soluble and exhibited a much higher brightness than the corresponding molecular dye (up to 10 fold).

In this article, we demonstrate the bio-imaging potential of these far-red emitting fluorescent polymer probes first *in cellulo* and then *in toto* using the zebrafish (*Danio rerio*). The latter has been largely validated as a valuable vertebrate model well suited for live imaging. Mainly, the zebrafish embryo exhibits overall tissue transparency and fertilization is external, which enables live imaging at all early embryonic stages. In a first step, we performed qualitative and quantitative cytotoxicity studies of the polymer probes in living cells. Then, we investigated their internalization pathway and extended the study to various human cell lines. We

also evaluated the resistance of the probes to photobleaching and showed that they can be advantageously used under two-photon excitation in the near-infrared for live cell imaging. Then, we demonstrated that such polymer probes were non-toxic to zebrafish embryos, efficiently diffused in the embryo depth and labeled sub-cellular structures, thus providing an efficient counterstain of tissues for live two-photon imaging.

2. Materials and methods

2.1. Synthesis of the polymer probes

The detailed synthesis of the fluorescent polymer probes has been described in a previous article [14].

2.2. UV-Visible absorption and fluorescence spectroscopy

UV-Visible spectra were recorded on a Jasco V-670 spectrophotometer at ambient temperature using 1 cm quartz cells. The fluorescence emission spectra were recorded using a Horiba-Jobin Yvon Fluorolog-3[®] spectrofluorimeter at 298 K, using a 1 cm quartz cells. The steady-state luminescence was excited by unpolarized light from a 450 W xenon CW lamp and detected at right angle (90°) for diluted solutions (DO < 0.1) by a red-sensitive Hamamatsu R928 photomultiplier tube.

2.3. Cell culture

Human HeLa cells used in this study were maintained in Dulbecco's modified essential medium (DMEM) supplemented with 10% fetal calf serum (FCS) and antibiotics (penicillin/streptomycin) [17]. Jurkat T cells (Human T cell leukemia cell line) were grown in RPMI-1640 medium (GIBCO) supplemented with glutamax, 10% FCS and antibiotics. The neuroblastoma cell line SH-SY5Y (ATCC # CRL-2266) was grown in a 1:1 mixture of Eagle Minimum essential medium (PAA E15-832) and F12 medium (PAA E15-890) supplemented with glutamax, 10% FCS and antibiotics. For differentiation studies, cells were treated for 4 days with retinoic acid (RA) at 10 μM in regular culture dishes, then transferred to chambered coverslips (μ -Slide 8 well, ibiTreat – 12,500 cells/well) and finally further differentiated with brain derived neurotrophic factor (BDNF) at 0.05 $\mu\text{g/ml}$ for 2–3 days. Prior live cell imaging, the medium was replaced with phenol red free medium to reduce autofluorescence.

In order to label specific cellular compartments, HeLa cells were transfected with plasmids expressing endosomal markers described elsewhere [17,18] 24 h prior to probe incubation.

2.4. Cytotoxicity assays

To evaluate polymer probe cytotoxicity, 0.5×10^5 Jurkat cells were plated on a 24 well plate (Corning 3524 Costar 24 Well Clear TC-Treated Microplates) and incubated at 37 °C with different concentrations of various polymer probes (solubilized in the cell culture medium MEM-alpha, PAA) during 7 h or 32 h (no polymer probe for the control experiment).

A qualitative evaluation was carried out using an inverted microscope Leica DM IRBE with a EB-CCD camera (C4880 Hamamatsu, Ichinocho, Japan) controlled by the HIPIK Software (Hamamatsu). The cell observations were performed using a 40x oil immersion objective lens and the images processed with ImageJ freeware.

A quantitative evaluation was performed using a BD FACS Canto II flow cytometer equipped with the BD FACS Diva Software (10,000 cells per condition). Cell viability was determined using the granulometry mode of the FACS system that distinguishes viable cells from granular non-viable cells.

2.5. Internalization assays

Cells were plated on chambered coverslips (μ -Slide 8 well, ibiTreat – 12,500 cells/well) and allowed to adhere overnight. In the case of the Jurkat T cells, cells were allowed to adhere on polylysinated coverslips 30 min prior to the addition of the polymer probe. Cells were then incubated for 1h30 to 2 h with different concentrations of polymer probes solubilized in the cell culture medium (MEM-alpha or RPMI). Cells were washed twice with PBS 1X to remove the residual (non internalized) polymer probe and visualized using inverted microscope LEICA DM14000 with an incubation chamber (CO₂ and temperature control), consisting of a confocal "spinning disk" head (Yokogawa CSU22), an EMCCD camera (Photometrics Quantem 512). This system is composed of 4 laser lights (405, 491, 561 and 635 nm) and controlled by the Metamorph Software (Molecular Devices). The cell observations were performed using the 63 \times water immersion objective lens (NA = 1.2). Generally, the exposition time was 800 ms. In the particular case of the Z-stacks, the exposition time was 1300 ms. Images were processed with ImageJ freeware.

2.6. Resistance to photobleaching assays

Cells were plated on chambered coverslips (μ -Slide 8 well, ibiTreat – 12,500 cells/well) and allowed to adhere overnight. They were then incubated for 3 h with the polymer probe (P3, 1 μM) and 1 h with the commercial probe LysoTracker[®] Red DND-99 (75 nm) solubilized in the cell culture medium (MEM-alpha, PAA). Cells

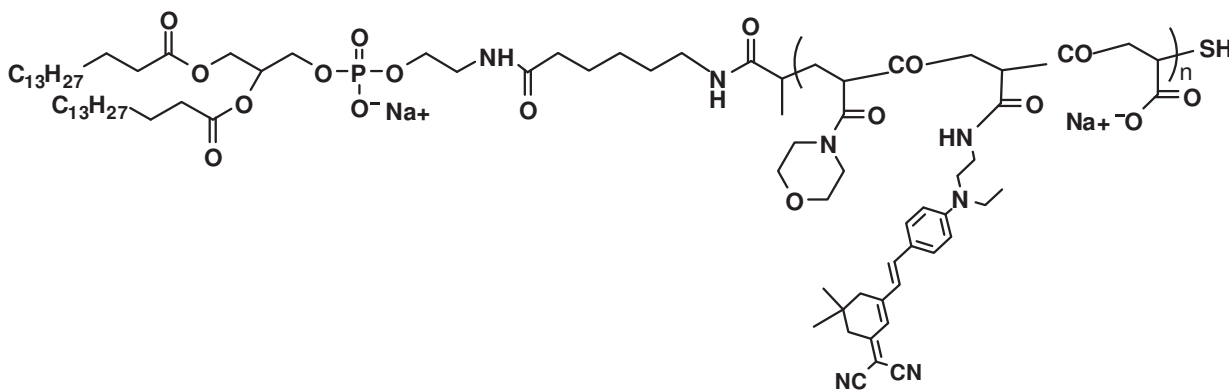


Fig. 1. Chemical structure of the far-red fluorescent polymer probes.

were washed twice with PBS 1X in order to remove the residual (non internalized) probe. Cells were illuminated in continuous mode (25% of the maximal power of the 200 W metal halid source of a HXP 200 C system) and images were recorded every 40 s using a microscope ZEISS Observer Z1 controlled by the AxioVision Software. The observations were performed using a 63 \times oil immersion objective lens (NA = 1.4). All images were processed with ImageJ freeware.

2.7. Two-photon live cell imaging

Cells were plated on chambered coverslips (μ -Slide 8 well, ibiTreat – 12,500 cells/well) and allowed to adhere overnight. They were then incubated for 15 h with 1 μ M of polymer probe P3 solubilized in the cell culture medium (MEM- α , PAA), washed twice with PBS 1X in order to remove the residual (non internalized) polymer probe and visualized using a ZEISS LSM780 (Carl Zeiss, Germany) confocal inverted microscope with a 63 \times oil immersion objective and an incubation chamber (CO₂ and temperature control). Two-photon excitation was performed with a tunable infrared Ti:Sapphire Chameleon Ultra λ s laser (690/1040 nm, Coherent Inc.). The laser had been carefully calibrated with a powermeter (PM-10 Thorlab) in order that the cells received a constant illumination power whatever the excitation wavelength in the range 690–1000 nm. Fluorescence was detected using the GaAsP spectral detector and images were processed with ImageJ freeware.

2.8. Two-photon live zebrafish embryo imaging

To avoid pigmentation, the nearly transparent Casper line [19] was used throughout experiments. Animals and embryos were reared and staged as previously described [20]. Embryos were collected at the one-cell-stage and raised in embryo medium (EM) solution containing different concentrations of polymer probe P1 (5 μ M, 10 μ M and 20 μ M) for up to the end of the hatching period (72 hpf (hours post fertilization)). We first investigated if the polymer probe was efficiently crossing the chorion. For that purpose, the probe's diffusion was compared in embryos that were de-chorionated mechanically (with the use of forceps at the one-cell stage) and in chorionated sibling embryos by incubated them in EM supplemented in the probe P1. Second, polymer probe toxicity was assessed by comparing either probe-labeled or control chorionated embryos throughout embryogenesis until hatching.

Before imaging, probe-labeled embryos were rinsed three times for five min in EM and kept in EM. Then, embryos were manually de-chorionated and placed in Teflon or 1% agarose molds depending on the stage. Embryos at 27 hpf were anesthetized in 0.05% (w/v) buffered tricaine methane sulfonate (MS222) before imaging procedure. All the investigations using the zebrafish model were carried out in compliance with the European and international guidelines on animal welfare (Directive 2010/63/EU).

All images were taken on a ZEISS LSM780 (Carl Zeiss, Germany) confocal microscope using a water-immersion objective (Nikon LWD 16x/0.85 NA). Two-photon

excitation was performed with a Chameleon XR femtosecond laser (Coherent Inc.). The average laser power measured at the level of the specimen was ranging from 8 to 30 mW. The fluorescence was detected using the GaAsP spectral detector with channels ranging from 410 nm to 695 nm for the excitation/emission spectral analysis and from 543 nm to 695 nm for all images presented. Images were processed using the ZEN software (Zeiss) and ImageJ freeware.

3. Results and discussion

3.1. Structural and optical characteristics of the far-red fluorescent polymer probes

The polymer probes have been synthesized by covalent binding of a far-red emitting fluorophore on a water-soluble and biocompatible polymer chain based on poly(*N*-acryloylmorpholine-*co*-*N*-acryloxysuccinimide), P(NAM-*co*-NAS), exhibiting numerous reactive sites along the chain [14]. The aim was to bind several fluorophores per chain to increase the brightness of the resulting probe, taking into account the solubility issues (the free dye was hydrophobic) and the inherent self-quenching phenomenon. Since after the binding step, the residual activated ester functions were hydrolyzed, several carboxylic functions (mostly in the carboxylate form at pH 7) appeared along the chain (40–76 carboxylate groups) (Fig. 1). The presence of such a large number of carboxylate groups per chain was expected to enhance water-solubility and to favour an extended conformation of the polymer probe due to electrostatic repulsions. Indeed, polymer probes possessing 4 to 11 fluorophores per chain (of 20,000 to 33,000 g mol⁻¹) were water-soluble and exhibited a limited fluorescence self-quenching phenomenon (Table 1).

These polymer probes exhibited a large fluorescence emission band in water (between 650 and 750 nm) in the far-red region (Fig. S1 in SI). Since the maximum absorption wavelength was 505 nm in aqueous phase, such polymer probes have a large Stokes shift which is of high interest for optical microscopy [21]. The brightness of the polymer probes has been determined from their molar extinction coefficient and their fluorescence quantum yield.

Table 1
Characteristics of the far-red fluorescent polymer probes.

Polymer probe sample	M_n of polymer backbone g mol ⁻¹ (\bar{D}) ^a	Average number of fluorophores per polymer chain ^b	Average fluorophore density ^c %	Brightness in water cm ⁻¹ mol ⁻¹ L
Free fluorophore	/	/	/	1300 ^d
P1	20,300 (1.04)	3.8	3.0	4500
P2	20,300 (1.04)	10.8	8.5	3500
P3	33,200 (1.11)	8.5	4.0	13,100

^a \bar{D} = polydispersity index, representative of the chain size distribution.

^b Determined by size exclusion chromatography (SEC) with a UV-Vis detector.

^c Number of fluorophores related to the total monomer units per polymer chain.

^d Determined in chloroform since the free fluorophore is not water-soluble.

In comparison with the free fluorophore, much higher brightness values were obtained (reaching a factor 10 for P3). We noticed that to get an optimized brightness, it was necessary to control both the number of fluorophores per chain and the polymer chain length (to limit the self-quenching phenomenon), i.e., it was preferable to remain below a fluorophore density of 4 mol% (in comparison with the total monomer units along the chain).

3.2. Evaluation of the cytotoxicity of the polymer probes

The aim of this study was to check that the polymer probes would not induce cell mortality at a usual concentration for such probes (around 1 μM [22]). First, a qualitative evaluation was carried out by wide field microscopy. The polymer probe P3 was incubated 2 days with HeLa cells at increasing concentrations: 0.1, 1, 10 and 20 μM . Microscopy images (Fig. S2 in SI) indicated that the cells kept their initial viability and morphology (no additional cell death as compared with a control experiment without probe) for probe concentration below 10 μM . At 20 μM , a higher number of dead cells were observed as cells became spherical and loose.

Then, a quantitative evaluation was performed by flow cytometry on non-adherent cells (Jurkat T lymphocytes). The three different polymer probes were incubated 7 or 32 h with the cells at increasing concentrations: 0.1, 1, 10 and 20 μM . Then, the percentage of living cells was determined by flow cytometry (granulometry mode) in comparison with a control experiment without probe (Fig. 2).

The results after 7 and 32 h incubation period confirmed the qualitative observations: for polymer probes P1 and P3 at concentrations below or equal to 10 μM , the percentage of living cells was the same as for the control. At 20 μM , a small decrease of the living cell percentage was noticed. Concerning polymer probe P2, it was not cytotoxic below 10 μM ; however, at 10 or 20 μM , a decrease of the living cell percentage was observed. This last polymer probe was bearing the highest fluorophore density (8.5 mol%, Table 1) and then was the less hydrophilic. This qualitative and quantitative cytotoxicity study confirmed that at micromolar probe concentrations (below 10 μM), the polymer probes were not cytotoxic on adherent and non-adherent human cells.

3.3. Influence of the polymer probe concentration on internalization and visualization

Some preliminary observations by wide field microscopy had shown that, after incubation with the polymer probe, the cells were fluorescent in the expected wavelength range which was a first indication of their labeling. To observe if the polymer probe was indeed internalized inside the cells, we then carried out fluorescence confocal microscopy. The question was: were the polymer probes internalized in living cells? if yes, what was the minimal

probe concentration in order to get a convenient intracellular visualization? The evaluation was performed on adherent human HeLa cells using the polymer probe samples P1, P2 and P3 at the same concentration (1 μM), as well as decreasing concentrations (0.5 and 0.2 μM) of polymer probe P3.

After a 2 h incubation of the three polymer probes with HeLa cells, image analysis indicated that all the cells were labeled (Fig. 3). Moreover, since the acquisition was performed on a confocal microscope, it showed that the probe was indeed internalized inside the cell and not adsorbed at the cell surface (see the Z-stack in Fig. S3 in SI). For polymer probes P1 and P3 (Fig. 3A and C), the contrast (signal over noise) was very good (low background noise without cell washing) which indicated that very few probes remained in the surrounding medium. In order to get an even better contrast, we generally performed one or two cell washes before image acquisition. For polymer probe P2 (Fig. 3B), some fluorescent aggregates were visible above the cells. This could be explained by its high fluorophore density that reduced its water-solubility. Consequently, polymer probe P2 was no longer considered and polymer probes P1 or P3 were used in the following studies.

The labeling distribution appeared similar for all cells with many very bright cytosolic spots, a diffuse labeling of the cytoplasm but no labeling of the nucleus. We could exclude the hypothesis of an intracellular precipitation of the probe since the bright spots were moving rapidly across the cytoplasm (determination of an average of 0.57 $\mu\text{m/s}$). Indeed, it was a first indication that the bright spots could correspond to endosomes trafficking along microtubules [23] (literature values around 0.5 $\mu\text{m/s}$) [24]. Moreover, the distribution of these bright spots in the cytoplasm was concentrated preferentially on one side of the nucleus. Such non-symmetrical labeling could correspond to an endosomal and/or MTOC (MicroTubule Organizing Center) localization. Conversely, the cytosolic diffuse labeling could be explained by a small fraction of the polymer probe being internalized by passive diffusion across the plasma membrane. Note that this intracellular probe labeling was reproducible with the three polymer probes.

Concerning the labeling intensity, cells appeared highly fluorescent after the two hour incubation with a probe concentration of 1 μM . When this concentration was decreased to 0.5 and 0.2 μM (Fig. 3D and E), the labeling was still conveniently visualized in all cells. The optimal polymer probe concentration was determined to be 0.5 μM (avoiding image saturation that could sometimes occur for 1 μM and above). Whatever the probe concentration, the intracellular probe localization was similar, with the presence of highly fluorescent spots in the cytosol surrounding the nucleus as well as a cytosolic diffuse labeling.

At this step, we could conclude that the polymer probes could efficiently label *living* adherent human cells such as HeLa cells at a

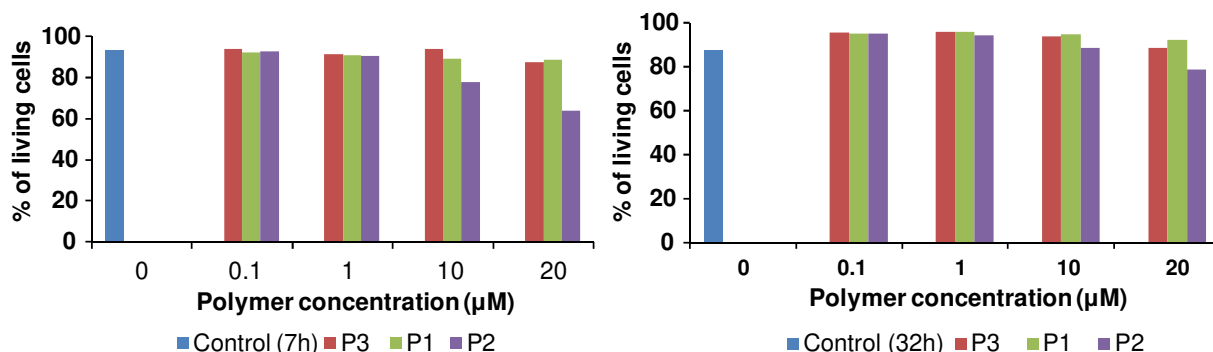


Fig. 2. Percentage of living cells (T lymphocytes) after 7 h (left) and 32 h (right) incubation with increasing concentrations of several polymer probes, assessed by flow cytometry.

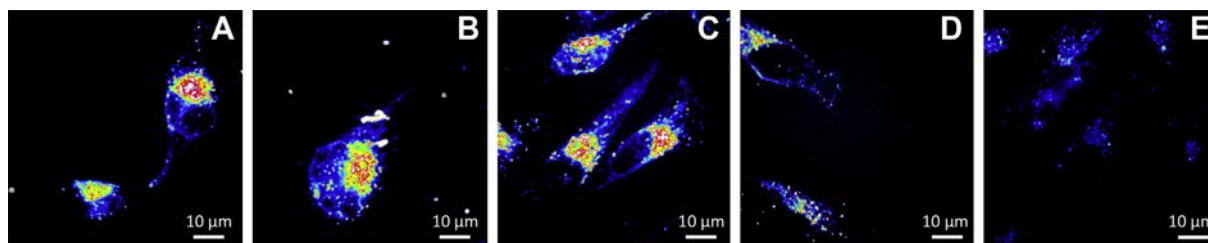


Fig. 3. Fluorescence confocal microscopy images after 2 h incubation with HeLa cells of polymer probes P1 (A), P2 (B) and P3 (C) at 1 μM , and decreasing concentrations of polymer probe P3: 0.5 μM (D) and 0.2 μM (E). Grey levels were color-coded with the 16 color look-up-table (LUT) from ImageJ. (For interpretation of the references to color in this figure legend, the reader is referred to the web version of this article.)

concentration as low as 0.2 μM . Contrary to many molecular probes, it was not necessary to use a carrier (such as a histone or a polyethyleneimine (PEI) cargo) to make the probe entering the cell, the polymer backbone itself being the nanocarrier. Moreover, the labeling was similar for all cells and seemed to proceed via endocytosis of the polymer probe from the plasma membrane.

3.4. Polymer probe internalization kinetics

To investigate the probe internalization step, we decided to follow the internalization kinetics by addition of the probe solution onto the cells directly under the confocal microscope. Image acquisition began after 10 min incubation of the probe (Fig. 4) instead of two hours as described previously. The corresponding images showed that it was already possible to visualize the fluorescent probe inside the cell 10 min after the probe addition. The

labeling intensity was increasing until 40 min and then remained unchanged.

In a complementary experiment, we investigated if cell washing would make the polymer probe being externalized out of the cells. Cells were incubated two hours with the polymer probe, then, replacement of the extra-cellular medium by fresh culture medium was performed. After this washing, the cells remained highly fluorescent indicating that the polymer probe was still largely present inside the cells. Even after additional washes (5 and 24 h after incubation), cells were still highly fluorescent, suggesting that the labeling was very stable, enabling long-term imaging.

3.5. Study of the polymer probe internalization pathway

To investigate if the polymer probe was indeed internalized in endosomes, a colocalization study was carried out between the

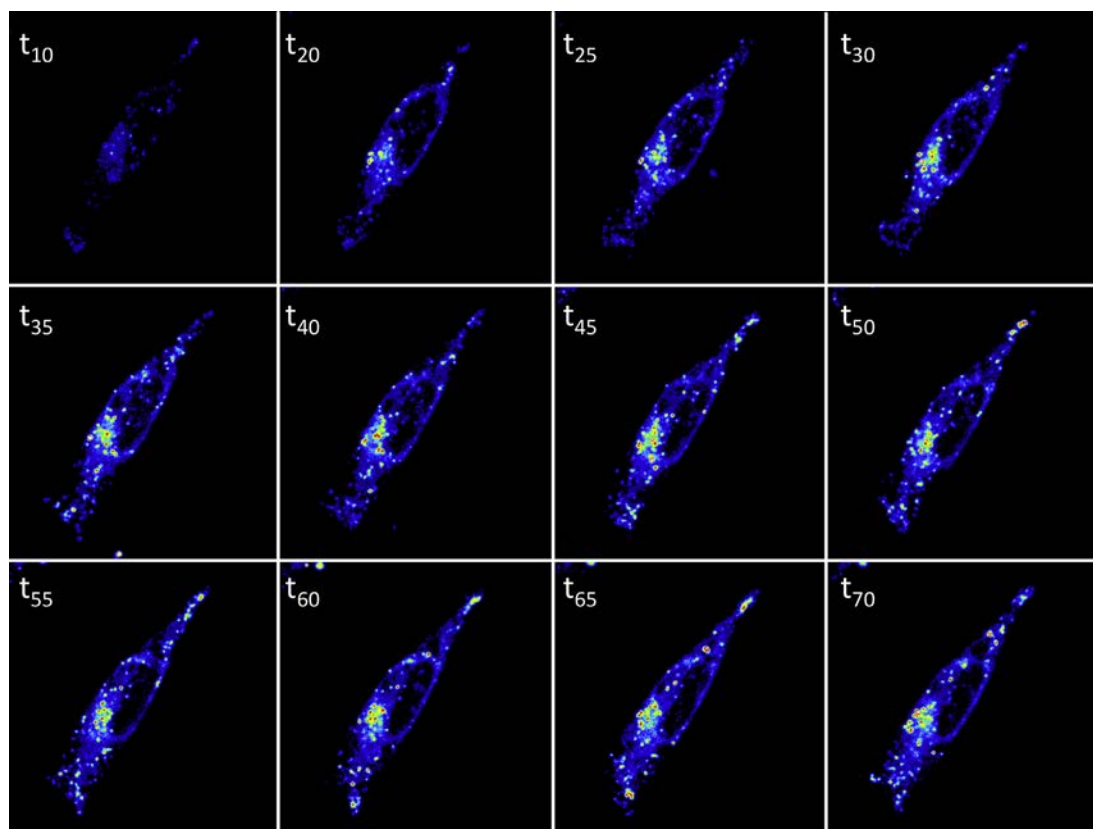


Fig. 4. Fluorescence confocal microscopy images after incubation of the polymer probe (P3, 1 μM) with HeLa cells (Images were recorded 10 min after the beginning of the probe incubation, then every five minutes). Grey levels were color-coded with the 16 color look-up-table (LUT) from ImageJ. (For interpretation of the references to color in this figure legend, the reader is referred to the web version of this article.)

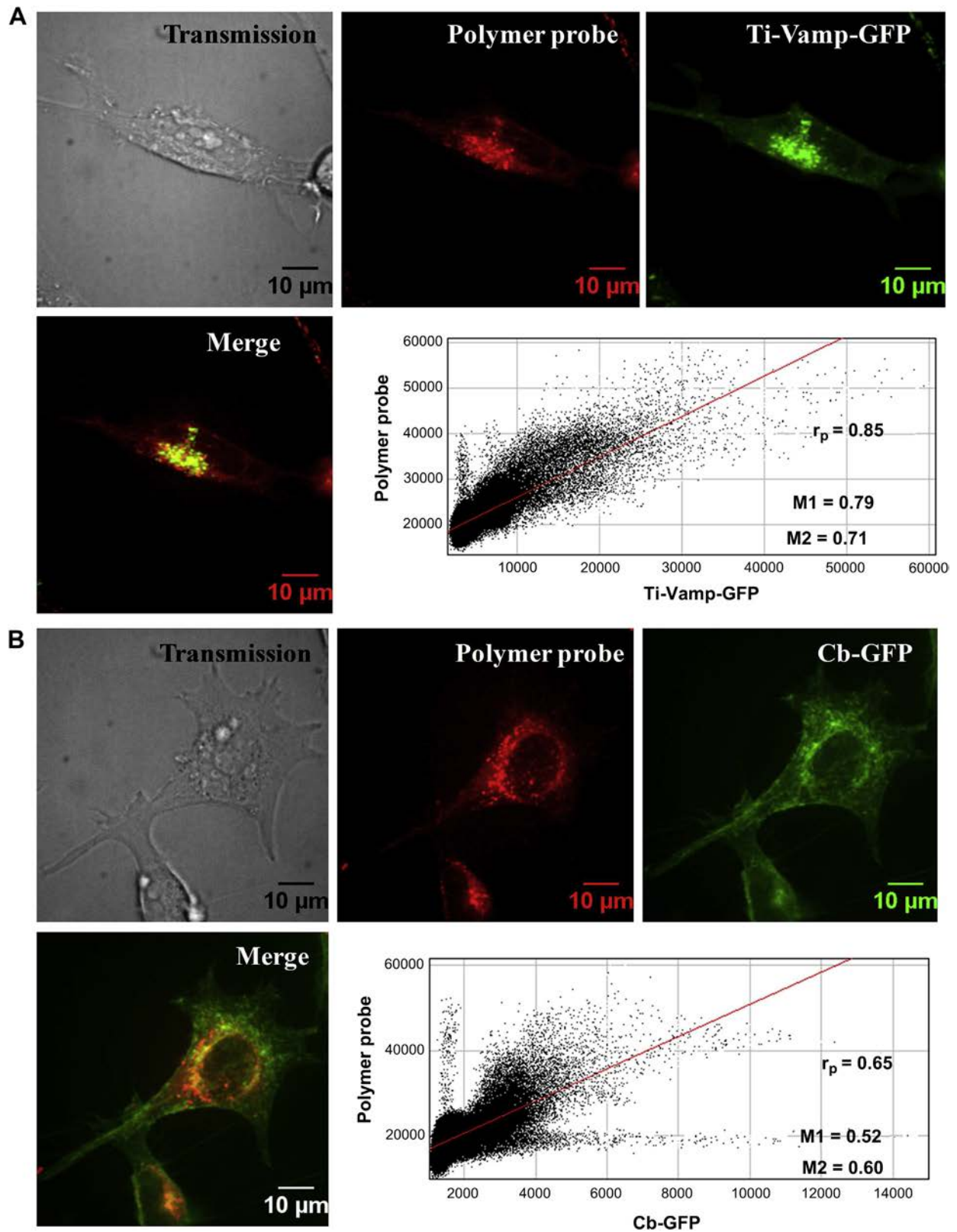


Fig. 5. Fluorescence confocal microscopy images after 2 h incubation of the polymer probe (P3, 0.5 μm) in HeLa cells expressing Ti-Vamp-GFP (A) or Cb-GFP (B). Top images: transmission (DIC mode) (left); polymer probe (middle); fluorescent proteins (right). Bottom: merge of red and green images; cytofluorogram with Pearson's coefficient, r_p , and Manders coefficients, M1 (% of green dots that colocalize with red dots) and M2 (% of red dots that colocalize with green dots). (For interpretation of the references to color in this figure legend, the reader is referred to the web version of this article.)

probe and endosomal markers. For that purpose, two different plasmids expressing fluorescent tagged endosomal proteins were chosen. The first one expressed the Tetanus neurotoxin Insensitive Vesicle-Associated Membrane Protein (Ti-Vamp) specifically present in late endosomes and playing an important role in their fusion with lysosomes [25,26]. The second one expressed the cellubrevin protein (Cb) specifically present in recycling endosomes that recycle membrane receptors (involved in receptor dependent endocytosis phenomena) from the plasma membrane [27,28]. Both recombinant proteins were labeled with the green fluorescent protein (GFP), which was chosen since its fluorescence emission was centered around 505 nm, away from the fluorescence emission of the polymer probe centered around 650 nm (in cells). A preliminary test showed that no fluorescence arising from GFP was detected in the red channel used for the polymer probe (675/67 nm).

HeLa cells were transfected by one or the other plasmid 24 h prior P3 polymer probe addition and image acquisition was performed by fluorescence confocal microscopy (Fig. 5). A qualitative analysis of the cytofluorograms (derived from the red and green images) based on the Pearson's coefficient [29], r_p , gave a first estimate of the colocalization, indicating a partial colocalization between both polymer probe/Ti-Vamp protein ($r_p = 0.85$) and polymer probe/cellubrevin ($r_p = 0.65$) (1 stands for a complete correlation and zero for no correlation). Then, a quantitative analysis based on the Manders coefficients [29], indicated that the percentage of the polymer probe that colocalized with Ti-Vamp protein reaches 71% ($M2 = 0.71$) against 60% with Cellubrevin,

thus illustrating that the polymer probe colocalized only a little bit more with late endosomes than with recycling endosomes. However, considering the M1 coefficients, the percentage of the endosomal markers that colocalized with the polymer probe showed a higher difference between both populations of endosomes. In fact, 79% of the late endosomes colocalized with the polymer probe, for only 52% of the recycling endosomes. This result suggests that the polymer probe traffics preferentially towards late endosomes, explaining the observed non-symmetrical distribution of the bright spots around the nucleus and supporting probable probe internalization from the plasma membrane via endocytosis.

3.6. Polymer probe internalization in various cell types

In order to check if internalization of the polymer probe was dependent upon the cell shape and cell line, the same labeling experiment was carried out in HeLa cells, T lymphocytes and neurons. Since T lymphocytes (Jurkat cells) are non-adherent cells, with a round shape and a very high membrane curvature, internalization of a probe might proceed differently than in HeLa cells (adherent, flat shape cells enriched in membranes). Neuronal cells (SH-SY5Y neuroblastoma) are also adherent cells. The behavior of the polymer probe in neuroblastoma cells was compared before and after differentiation since differentiated cells could exhibit a different endocytotic or membrane trafficking activity [30]. In addition, neuroblastoma cells exhibit a wide plasma membrane surface due to neurite outgrowth. The various cell lines were

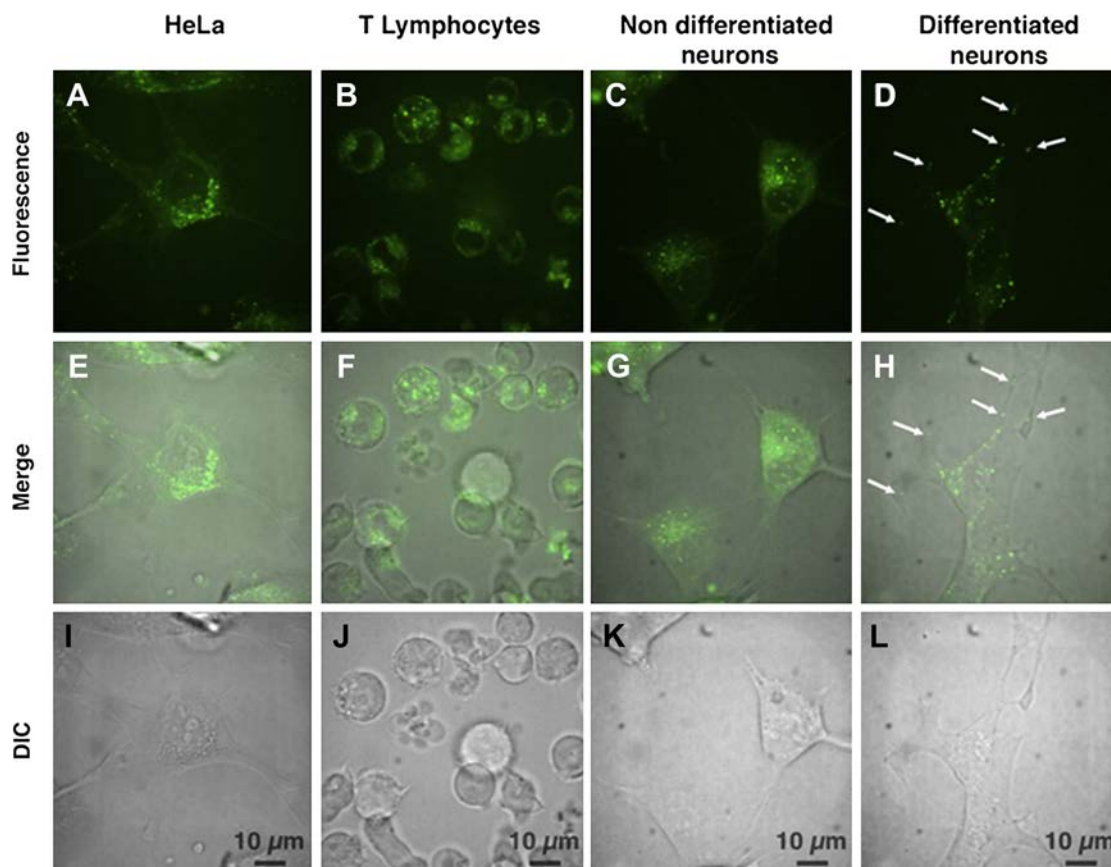


Fig. 6. Fluorescence confocal microscopy images taken on live cells after 30 min to 1 h incubation of the polymer probe (P3). HeLa cells (A, E, I, 1 μm of P3), T lymphocytes (B, F, J, 1 μm), non-differentiated neurons (C, G, K, 1 μm) and differentiated neurons (D, H, L, 0.5 μm) are displayed. The cells are visualized in grey by transmission (DIC mode) on E–L panels. Fluorescent images (visualized in green, false color) are presented separately on A–D and superimposed with corresponding transmission images on E–H. White arrows indicate the presence of bright spots inside neurites (D and H). (For interpretation of the references to color in this figure legend, the reader is referred to the web version of this article.)

incubated with polymer probe P3 (for 30 min to 1 h) and visualized by fluorescence confocal microscopy (Fig. 6).

In each case, a high labeling of the cells was noticed at short observation times (5–10 min) indicating a fast internalization of the polymer probe. Moreover, the probe localization was similar in all cells, with a diffuse cytosolic labeling and numerous bright spots in the cytoplasm concentrated on one side of the nucleus, moving rapidly across the cytoplasm (around $0.62 \mu\text{m/s}$ for T cells). In differentiated neurons, bright spots were not only present around the cell nucleus (like in non-differentiated cells) but were also found along neurites (see arrows on Fig. 6D and H) thus indicating that the polymer probe can localize in neurites in neuronal cells. This comparative study indicated that the cell internalization of polymer probe P3 did not seem to be cell line nor proliferation nor differentiation nor shape dependent and strongly suggested that it preferentially occurred via endocytosis, as shown in HeLa cells.

3.7. Resistance of the polymer probe to photobleaching

When considering a new probe, one characteristic especially relevant for optical microscopy is its resistance to photobleaching. Often, molecular dyes as well as fluorescent proteins (like green fluorescent protein, GFP) undergo a fast photobleaching. Then, we decided to investigate the *in cellulo* kinetics of photobleaching of polymer probe P3 under a constant light illumination (200 W metal halide source). The polymer probe was compared to a well-known commercial molecular probe, the LysoTracker[®] Red (DND-99). This latter probe was chosen since it emits in the red spectral range like our polymer probe and since it is a marker of endosomes and lysosomes [31,32]. DND-99 leads to a similar labeling distribution in living cells than the polymer probe: a diffuse cytosolic labeling and numerous bright spots close to the nucleus. The two probes were used at their optimal concentration for a convenient visualization. Cells were illuminated under a continuous mode in conditions chosen to be representative of usual observations by optical microscopy: 25% of the maximal power of the light source.

For each probe, two regions of interest (ROI) were chosen: inside the cell in a bright area (signal) and outside the cell in a dark area (noise). Then, the signal/noise ratio was reported for each probe (after normalization) versus illumination time (Fig. 7). With DND-

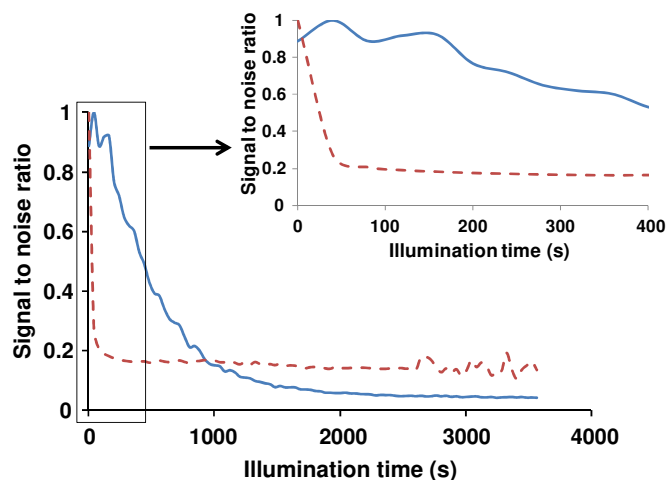


Fig. 7. *In cellulo* kinetics of photobleaching: Normalized fluorescence emission (signal to noise ratio) versus illumination time (constant illumination, 25% power of the white source), after incubation with HeLa cells of either the polymer probe P3 (full line, $1 \mu\text{M}$, 3 h incubation) or the LysoTracker[®] Red probe (dashed line, 75 nM, 1 h incubation) and two washes.

99 probe, the fluorescence half-lifetime, $t_{1/2}$, is lower than 40 s whereas for the polymer probe, the $t_{1/2}$ is 400 s. Therefore, under the same observation conditions, our polymer probe is at least 10 fold more resistant to photobleaching than the LysoTracker[®] Red DND-99 probe, making it promising for time-lapse tracking studies.

3.8. Two-photon microscopy live cell imaging

Since the fluorophore used to label the polymer is a conjugated push–pull dipolar molecule, it was expected to possess efficient two-photon absorption (TPA) properties. As the binding of the fluorophore onto PNAM-based copolymers resulted in water-soluble polymer probes, it was possible to investigate their TPA properties in biological medium.

After incubation of P3 polymer probe with HeLa cells, it was possible to visualize the cells under two-photon excitation on a large range of NIR excitation wavelengths (λ_{EX} from 750 to 1000 nm) (Fig. 8). The fluorescence emission was collected at 652/44 nm since the *in cellulo* fluorescence emission spectrum exhibited a $\lambda_{\text{EM max}}$ at 650 nm. In a control experiment without polymer probe (only cells, not shown) run in the same conditions and for the same illumination power (at $\lambda_{\text{EX}} = 750 \text{ nm}$), we did not record any fluorescence that could correspond to autofluorescence (for instance, from NADH/NADPH present in cell mitochondria) [33,34]. The *in cellulo* two-photon excitation spectrum of polymer probe P3 was then reconstructed from 750 nm to 1000 nm (every 10 nm), using the average fluorescence intensity emitted at 652/44 nm on each image (Fig. 9).

This two-photon excitation spectrum *in cellulo* exhibited a maximum around 920 nm (Fig. 9 – inset). It is worth noting that, for a star-shaped oligomer probe based on the same chromophore, a two-photon absorption study *in aqueous phase* had indicated a peak between 900 and 1070 nm (with a maximum around 1050 nm) [35]. This behavior is in good agreement with the red shift of the polymer probe fluorescence band observed *in water* with respect to that *in cellulo* (Fig. 10). It is possible that, *in cellulo*, variations of the micro-environment around the polymer probes inside endosomes induce the formation of some dye aggregates that would influence spectroscopic properties. Such variations could arise from pH changes (pH is usually more acidic in endosomes) that would decrease the polarity of the polymer backbone or from an increase of the local probe concentration during endosomal sequestration.

In addition, very strong fluorescence emission intensity was observed below 800 nm excitation wavelength, with a strong enhancement for 700–750 nm excitation (saturation of the images, in agreement with the excitation spectrum on Fig. 9). Note that the laser had been carefully calibrated in order that the cells received a constant illumination power whatever the excitation wavelength in the range of 690–1000 nm. Such an observation illustrates a higher TPA cross-section value at shorter wavelengths than those corresponding to the lowest excited state exhibiting a maximum around 920 nm under two-photon excitation (Fig. 9 and Fig. S4 in SI). This behavior has already been observed for numerous other chromophores (for instance fluorescein) [36].

Finally, this study confirmed that the polymer probe can lead to very convenient two-photon imaging of living cells, with two-photon excitation in the NIR (750–950 nm) and fluorescence emission in the far-red (650 nm). Since NIR excitation presents several advantages for bio-imaging such as a lower light-induced cytotoxicity, a reduced autofluorescence and a deeper tissue penetration, such polymer probes might be valuable tools for *in vivo* imaging studies. This was further evaluated in zebrafish embryos.

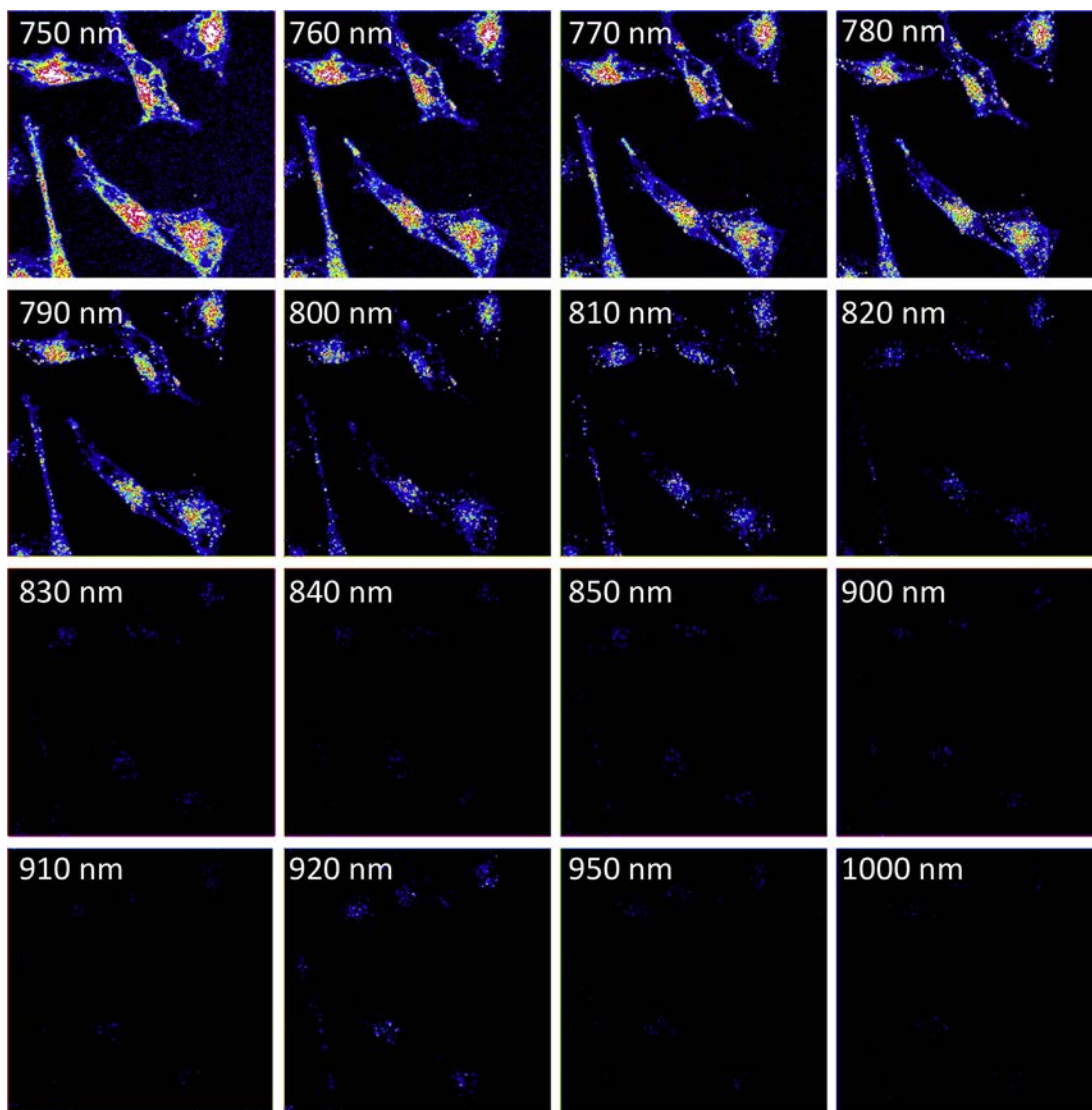


Fig. 8. Laser scanning fluorescence microscopy images under two-photon excitation at various λ_{EX} , after incubation of the polymer probe P3 ($1 \mu\text{M}$) in HeLa cells for 15 h (collected at 652/44 nm). Grey levels were color-coded with the 16 color look-up-table (LUT) from ImageJ. (For interpretation of the references to color in this figure legend, the reader is referred to the web version of this article.)

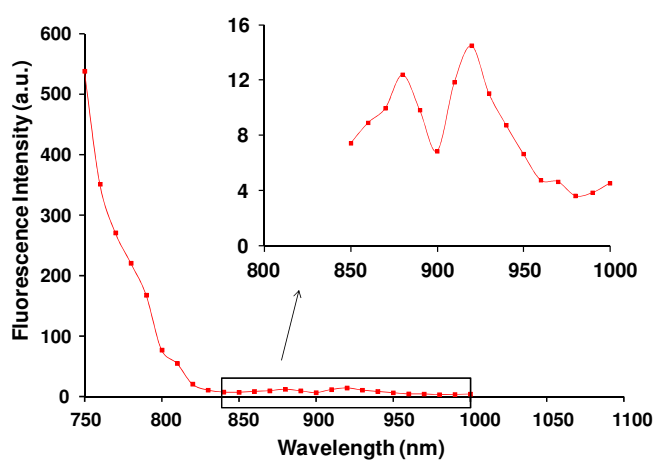


Fig. 9. *In cellulo* two-photon excitation spectrum (emission collected at 652/44 nm) after incubation of the polymer probe P3 ($1 \mu\text{M}$) in HeLa cells for 15 h.

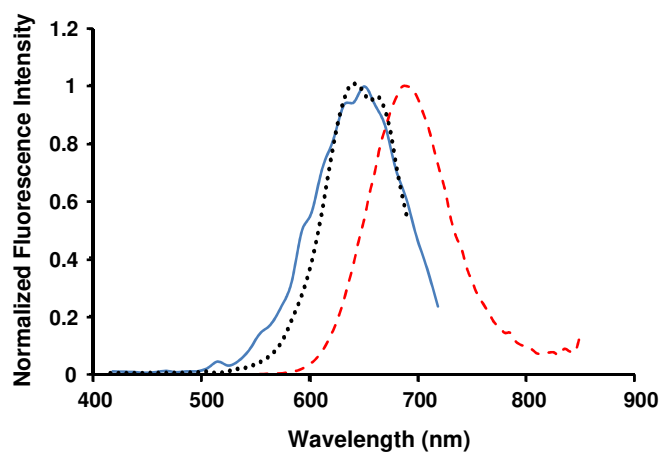


Fig. 10. Comparison of the fluorescence emission spectra of the polymer probe: *in toto* after 75 min incubation with zebrafish embryo (dotted line, $5 \mu\text{M}$, $\lambda_{EX} = 514 \text{ nm}$), *in cellulo* after 1 h incubation with HeLa cells (full line, $1 \mu\text{M}$, $\lambda_{EX} = 488 \text{ nm}$) and in water in a spectroscopy cuvette (dashed line, $0.5 \mu\text{M}$, $\lambda_{EX} = 510 \text{ nm}$).

3.9. Study of the polymer probe internalization and cytotoxicity in zebrafish embryos

Numerous applications using zebrafish embryos as a vertebrate model organism involve a vast selection of fluorescent probes like fluorescent proteins, inorganic probes and organic probes [37]. However, the expression of fluorescent proteins requires various manipulations such as RNA or DNA injection and only provides enough signal after several hours of delay depending on the biosynthetic machinery. Concerning the inorganic fluorescent probes like quantum dots (QD), they have limited application for zebrafish imaging because of potential toxicity and *in toto* delivery issues [38]. Then, there is a great need for organic probes, organism-permeable and crossing the chorion (an acellular envelope surrounding the zebrafish embryo). Emission in the far-red range (limiting detection of autofluorescence) and high TPA efficiency in the near-infrared (enabling deep tissue imaging and reducing photodamages around the focal point) are other desirable properties for zebrafish embryo imaging. From the cell culture experiments, we expected the polymer probes to be efficient *in toto* labeling reagents for live zebrafish embryos.

The internalization and biocompatibility were investigated by bathing one-cell stage zebrafish embryos with different concentrations of polymer probe P1 for various periods of time (experimental section). We first observed that the probe crossed the chorion and stained the embryonic cells. We compared the diffusion of the probe P1 (at 5 μM , 10 μM or 20 μM) in embryos that were mechanically de-chorionated (at the one-cell stage) and in chorionated embryos. The diffusion of the probe was similar in time and depth in both kinds of embryos as confirmed by two-photon imaging of embryos at 5 h post fertilization (hpf). This result demonstrates that the polymer probe is efficiently crossing the chorion and moreover diffuses rapidly through the depth of the embryo. Then, the use of such polymer probe does not require a prior de-chorionation procedure which is delicate and time consuming especially at early developmental stages. We further observed that after bathing 24 hpf embryos (about 2.5 mm long) as short as 75 min in 5 μM probe solution, full labeling through the whole depth of the specimens (200–500 μm) was achieved.

These experiments also revealed that the polymer probe was non-toxic to developing zebrafish embryos even when incubated in 20 μM solution from the one-cell stage until hatching by 48 hpf. Probe-labeled larvae hatched normally compared to non-labeled ones with no significant lethality nor abnormality or delayed development. These results demonstrated the biocompatibility of polymer probe P1 and its convenience for staining zebrafish embryonic tissues as it appeared to cross the chorion barrier whatever the developmental stage, at least up to 48 hpf.

In addition, we recorded the *in toto* fluorescence emission spectrum of the polymer probe and compared it with the *in cellulo* one. The spectra were very similar and, in both cases, exhibited a maximum in the far-red range around 650 nm (full and dotted lines, Fig. 10). In comparison, the emission spectrum of the polymer probe in water (recorded by fluorescence spectroscopy) was red-shifted (dashed line, maximum at 690 nm). For a dye derivative having the same chromophoric core, an important solvatochromic effect had already been shown [35]. In fact, upon increasing solvent polarity, the emission peak was more and more red-shifted (maximum from 630 nm in dioxane to 676 nm in water, positive solvatochromism). Such a behavior seemed to indicate that, in both HeLa and zebrafish embryonic cells, the polymer probe was mainly located in regions of low polarity like the lipid bilayer of endosomes.

3.10. *In vivo* two-photon microscopy imaging of live zebrafish embryos

The emission-excitation spectra of polymer probe P1 in the zebrafish embryonic cells were explored by two-photon excitation in the range 705–980 nm and detection between 410 and 695 nm (with a GaAsP spectral detector). Similarly to the *in cellulo* experiments, the probe P1 exhibited two excitation maxima, a major one around 700–750 nm and a smaller one around 910 nm. However, for a two-photon excitation wavelength of 750 nm, some autofluorescence was detected in the control embryo due to the presence of NADH/NADPH and other intracellular components (Fig. 11A). On the contrary, for a two-photon excitation wavelength of 910 nm, no autofluorescence was detected in the control embryo while the P1-labeled embryo exhibited strong fluorescence signal (Fig. 11B).

Then, for *in vivo* imaging of 5 hpf and 27 hpf embryos, an excitation wavelength of 910 nm was chosen and the fluorescence emission was collected in the range 543–695 nm. Staining was observed in the cytoplasm of all the embryonic cells and was distributed in a dotted pattern similar to the one described for the *in cellulo* experiments, suggesting that the polymer probe was indeed internalized most probably through the endosomes (Fig. 12A and B). Moreover, fluorescence was still high in the cytoplasm of the cells throughout the embryo 24 h post-staining, demonstrating that the probe achieved long-term stable *in toto* staining of zebrafish embryonic cells (Fig. 12C and D). Polymer probe enabled imaging of the somites and overlying epidermis of the 27 hpf embryo tail (close-up view in D). With its innocuity, ability to cross the chorion and to rapidly penetrate the depth of embryonic tissues, the polymer probe appeared as a useful counterstain for two-photon imaging of live zebrafish embryos with an interesting emission spectrum in the far-red range.

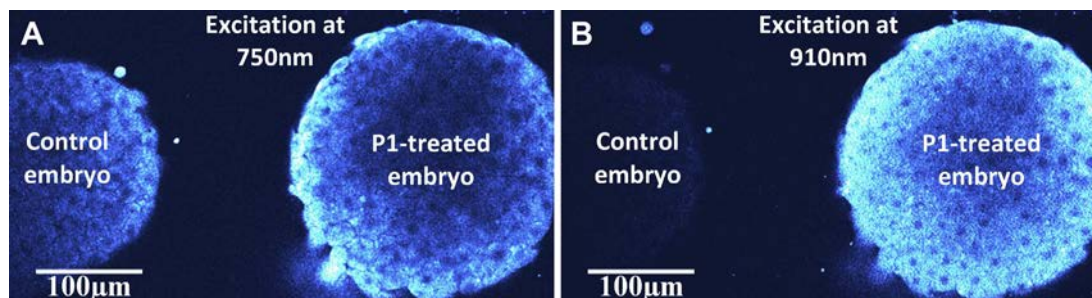


Fig. 11. Optimization of the polymer probe P1 signal to noise ratio. (A,B) Two-photon imaging of control embryos (left in each image) and probe-labeled embryos raised in EM supplemented with 5 μM of polymer probe P1 until imaging (right in each image). Two-photon excitation (A) at 750 nm (8 mW) and (B) at 910 nm (30 mW). Grey levels were color-coded with the cyan hot look-up-table (LUT) from ImageJ. (For interpretation of the references to color in this figure legend, the reader is referred to the web version of this article.)

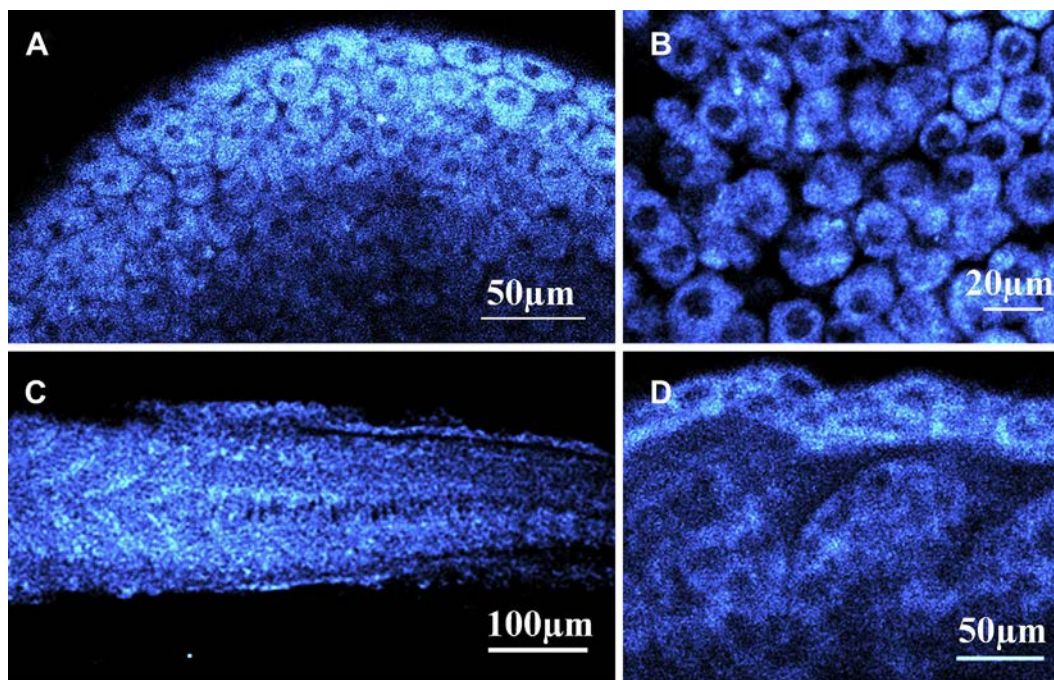


Fig. 12. Two-photon imaging of zebrafish live embryos. Embryos were incubated in embryo medium containing 5 μM of polymer probe P1 for 75 min, then rinsed and raised in embryo medium until imaging. Excitation wavelength, $\lambda_{\text{Ex}} = 910$ nm, fluorescence emission was collected in the range 543–695 nm. (A, B) Embryo at the 5 hpf. Polymer probe is detected through the blastoderm depth and is localized in the cytoplasm of the cells (close-up view in B). (C, D) Tail of a 27 hpf embryo. Polymer probe P1 is still detected in the cytoplasm of the cells throughout the embryo 24 h post-staining, as shown in the somites and overlying epidermis (close-up view in D). Grey levels were color-coded with the cyan hot look-up-table (LUT) from ImageJ. (For interpretation of the references to color in this figure legend, the reader is referred to the web version of this article.)

4. Conclusions

The biological evaluation of water-soluble polymer probes (emitting in the far-red range and expected to be efficiently excited in the NIR in the two-photon mode) has been carried out by flow cytometry and fluorescence confocal microscopy, first on living cells and then on zebrafish embryos as vertebrate model (requiring deep tissue imaging).

First, flow cytometry studies revealed that the polymer probes were not cytotoxic at concentrations up to 10 μM (after incubation of the probes for 7 and 32 h with T lymphocytes). Second, these polymer probes could efficiently label *living* HeLa cells, T lymphocytes and neurons. The labeling was similar for all cells (with a diffuse cytosolic labeling and the presence of numerous bright spots in the cytoplasm mostly located on one side of the nucleus). A colocalization experiment confirmed that internalization proceeded mainly by endocytosis of the polymer probe. Cells were still highly fluorescent several hours after incubation (even after several washes). Such a property could enable imaging studies that require a stable probe labeling during several hours.

Moreover, these polymer probes exhibited a high resistance to photobleaching in usual microscopy conditions, with a half-lifetime 10 fold higher than that of a commercial molecular probe. Then, these polymer probes appear useful for continuously following an intracellular dynamic process as well as for molecule or endosome tracking studies. In addition, the polymer probes were efficiently used for two-photon imaging of living cells, with two-photon excitation in the NIR (750–950 nm) and fluorescence detection in the far-red (650–750 nm). Thus, such polymer probes should be valuable tools for *in vivo* imaging studies. It was demonstrated in zebrafish embryos where the polymer probe exhibited remarkable properties in terms of biocompatibility, internalization, diffusion, stability, wavelength range and Stokes shift compared to other valuable organic probes [39]. The two-photon absorption peak at

910 nm is particularly interesting since it does not excite the zebrafish endogenous fluorescence and is likely to enable long-term time-lapse imaging with limited photodamage. Moreover, some recent data (unpublished results) showed that these polymer probes are also valuable *in vivo* imaging tools for other aquatic models like ascidia. We are then undertaking further investigations taking advantage of the polymer probe to study several biological issues such as the notochord formation.

Acknowledgments

We acknowledge the contribution of the cytometry platform and of the imaging facility platform (Claire Lionet and Christophe Chamot at PLATIM) (Biosciences Gerland-Lyon Sud, UMS3444, US8). We acknowledge Dr Yann Bretonnière (Laboratoire de Chimie, ENS) for help with the spectroscopic measurements and for fruitful discussions during this whole research project. We acknowledge Dr Cyrille Monnereau (Laboratoire de Chimie, ENS) and Professor Marek Samoc for interesting discussions about the *in cellulo* two-photon results. We acknowledge Baptiste Panthu (Unité de Virologie Humaine) and Xavier Gaume (Laboratoire Joliot-Curie) for the gift of HeLa cells. We acknowledge Timothée Bresson (Laboratoire Joliot-Curie) for the UV-Vis spectrum of Fig. S4. SA acknowledges a PhD grant from the Région Rhône-Alpes, Cluster 5 Chimie. We also thank the Fondation Innovations en Infectiologie (FINOVI) for funding (2009) and the CNRS for an interdisciplinary program funding (PIRO51). Contribution by SB and NP was funded by FBI ANR-10-INBS-04-05 and zebrafish live imaging by the Bio-Emergences platform <http://www.bioemergences.eu>.

Appendix A. Supplementary data

Supplementary data related to this article can be found at <http://dx.doi.org/10.1016/j.biomaterials.2014.12.026>.

References

- [1] Tsien RY. Fluorescent probes of cell signaling. *Annu Rev Neurosci* 1989;12:227–53.
- [2] Pansare V, Hejazi S, Faenza W, Prud'homme RK. Review of long-wavelength optical and NIR imaging materials: contrast agents, fluorophores and multifunctional nano carriers. *Chem Mater* 2012;24:812–27.
- [3] Monici M. Cell and tissue autofluorescence research and diagnostic applications. *Biotechnol Annu Rev* 2005;11:227–56.
- [4] Andresen V, Alexander S, Heupel WM, Hirschberg M, Hoffman RM, Friedl P. Infrared multiphoton microscopy: subcellular-resolved deep tissue imaging. *Curr Op Biotech* 2009;20:54–62.
- [5] Musyanovych A, Schmitz-Wienke J, Mailänder V, Walther P, Landfester K. Preparation of biodegradable polymer nanoparticles by miniemulsion technique and their cell interactions. *Macromol* 2008;8:127–39.
- [6] Liu Y, Ogawa K, Schanze KS. Conjugated polyelectrolytes as fluorescent sensors. *J Photochem Photobiol C* 2009;10:173–90.
- [7] Li BK, Pan J, Feng S-S, Wu AW, Pu K-Y, Liu Y, et al. Generic strategy of preparing fluorescent conjugated-polymer-loaded poly(DL-lactide-co-glycolide) nanoparticles for targeted cell imaging. *Adv Funct Mater* 2009;19:3535–42.
- [8] Wu C, Bull B, Szymanski C, Christensen K, McNeill J. Multicolor conjugated polymer dots for biological fluorescence imaging. *ACS Nano* 2008;2:2415–23.
- [9] Dubé D, Francis M, Leroux J-C, Winnik FM. Preparation and tumor cell uptake of poly(*N*-isopropylacrylamide) folate conjugates. *Bioconjugate Chem* 2002;13:685–92.
- [10] Relogio P, Bathfield M, Haftek-Terreau Z, Beija M, Favier A, Giraud-Panis M-J, et al. Biotin-end-functionalized highly fluorescent water-soluble polymers. *Polym Chem* 2013;4:2968–81.
- [11] Wu C, Hansen SJ, Hou Q, Yu J, Zeigler M, Jin Y, et al. Design of highly emissive polymer dot bioconjugates for in vivo tumor targeting. *Angew Chem Int Ed* 2011;50:3430–4.
- [12] Lucas B, Remaut K, Sanders NN, Braeckmans K, De Smedt SC, Demeester J. Studying the intracellular dissociation of polymer-oligonucleotide complexes by dual color fluorescence fluctuation spectroscopy and confocal imaging. *Biochemistry* 2005;44:9905–12.
- [13] Saad M, Garbuzenko OB, Ber E, Chandna P, Khandare JJ, Pozharov VP, et al. Receptor targeted polymers, dendrimers, liposomes: which nanocarrier is the most efficient for tumor-specific treatment and imaging? *J Control Release* 2008;130:107–14.
- [14] Adjili S, Favier A, Massin J, Bretonnière Y, Lacour W, Lin Y-C, et al. Synthesis of multifunctional lipid-polymer conjugates: application to the elaboration of bright far-red fluorescent lipid probes. *RSC Adv* 2014;4:15569–78.
- [15] Massin J, Dayoub W, Mulatier C, Aronica C, Bretonnière Y, Andraud C. Near-infrared solid-state emitters based on isophorone: synthesis, crystal structure and spectroscopic properties. *Chem Mater* 2011;23:862–73.
- [16] Cepraga C, Gallavardin T, Marotte S, Lanoë PH, Mulatier J-C, Lerouge F, et al. Biocompatible well-defined chromophore-polymer conjugates for photodynamic therapy and two-photon imaging. *Polym Chem* 2013;4:61–7.
- [17] Grigorov B, Décimo D, Smagulova F, Péchoux C, Mougel M, Muriaux D, et al. Intracellular HIV-1 Gag localization is impaired by mutations in the nucleocapsid zinc fingers. *Retrovirology* 2007;4:54–65.
- [18] Grigorov B, Arcanger F, Roingard P, Darlix J-L, Muriaux D. Assembly of infectious HIV-1 in human epithelial and T-lymphoblastic cell lines. *J Mol Biol* 2006;359:848–62.
- [19] White RM, Sessa A, Burke C, Bowman T, LeBlanc J, Ceol C, et al. Transparent adult zebrafish as a tool for in vivo transplantation analysis. *Cell Stem Cell* 2008;2:183–9.
- [20] Kimmel CB, Ballard WW, Kimmel SR, Ullmann B, Schilling TF. Stages of embryonic development of the zebrafish. *Dev Dyn* 1995;203:253–310.
- [21] Baathulaa K, Xu Y, Qian X. Unusual large Stokes shift and solvatochromic fluorophore: synthesis, spectra and solvent effect of 6-substituted 2,3-naphthalimide. *J Photochem Photobiol A* 2010;216:24–34.
- [22] Pagano RE, Watanabe R, Wheatley C, Chen C-S. Use of N-[5-(5,7-dimethyl boron dipyrromethene difluoride-sphingomyelin to study membrane traffic along the endocytic pathway. *Chem Phys Lipids* 1999;102:55–63.
- [23] Gruenberg J, Maxfield FR. Membrane transport in the endocytic pathway. *Curr Opin Cell Biol* 1995;7:552–63.
- [24] Lebrand C, Corti M, Goodson H, Cosson P, Cavalli V, Mayran N, et al. Late endosome motility depends on lipids via the small GTPase Rab7. *EMBO J* 2002;21:1289–300.
- [25] Chaineau M, Danglot L, Galli T. Multiple roles of the vesicular-SNARE TI-VAMP in post-Golgi and endosomal trafficking. *FEBS Lett* 2009;583:3817–26.
- [26] Danglot L, Chaineau M, Dahan M, Gendron M-C, Boggetto N, Perez F, et al. Role of TI-VAMP and CD82 in EGFR cell-surface dynamics and signaling. *J Cell Sci* 2010;123:723–35.
- [27] Galli T, Chilcote T, Mundigl O, Binz T, Niemann H, De Camilli P. Tetanus toxin-mediated cleavage of cellubrevin impairs exocytosis of transferrin receptor-containing vesicles in CHO cells. *J Cell Biol* 1994;125:1015–24.
- [28] Fader CM, Sánchez DG, Mestre MB, Colombo MI. TI-VAMP/VAMP7 and VAMP3/cellubrevin: two v-SNARE proteins involved in specific steps of the autophagy/multivesicular body pathways. *Biochim Biophys Acta* 2009;1793:1901–16.
- [29] Bolte S, Cordelières FP. A guided tour into subcellular colocalization analysis in light microscopy. *J Microsc* 2006;224:213–32.
- [30] Selinummi J, Sarkanen J-R, Niemistö A, Linne M-L, Ylikomi T, Yli-Harja O, et al. Quantification of vesicles in differentiating human SH-SY5Y neuroblastoma cells by automated image analysis. *Neurosci Lett* 2006;396:102–7.
- [31] Lemieux B, Percival MD, Falgoutier J-P. Quantitation of the lysosomotropic character of cationic amphiphilic drugs using the fluorescent basic amine red DND-99. *Anal Biochem* 2004;327:247–51.
- [32] Nadanaciva S, Lu S, Gebhard DF, Jessen BA, Pennie WD, Will Y. A high content screening assay for identifying lysosomotropic compounds. *Toxicol In Vitro* 2011;25:715–23.
- [33] Chance B, Schoener B, Oshino R, Itshak F, Nakase Y. Oxidation-reduction ratio studies of mitochondria in freeze-trapped samples. NADH and flavoprotein fluorescence signals. *J Biol Chem* 1979;254:4764–71.
- [34] Zeng Y, Yan B, Sun Q, The SK, Zhang W, Wen Z, et al. Label-free in vivo imaging of human leukocytes using two-photon excited endogenous fluorescence. *J Biomed Opt* 2013;18:040504.
- [35] Massin J, Charaf-Eddin A, Appaix F, Bretonnière Y, Jacquemin D, van der Sanden B, et al. A water soluble probe with near infrared two-photon absorption and polarity-induced fluorescence for cerebral vascular imaging. *Chem Sci* 2013;4:2833–43.
- [36] Makarov NS, Drobizhev M, Rebane A. Two-photon absorption standards in the 550–1600 nm excitation wavelength range. *Opt Express* 2008;16:4029–47.
- [37] Ko SK, Chen X, Yoon J, Shin I. Zebrafish as a good vertebrate model for molecular imaging using fluorescent probes. *Chem Soc Rev* 2011;40:2120–30.
- [38] Tang S, Cai Q, Chibli H, Allagada V, Nadeau JL, Mayer GD. Cadmium sulfate and CdTe-quantum dots alter DNA repair in zebrafish (*Danio rerio*) liver cells. *Toxicol Appl Pharm* 2013;272:443–52.
- [39] Cooper MS, Szeto DP, Sommers-Herivel G, Topczewski J, Solnica-Krezel L, Kang HC, et al. Visualizing morphogenesis in transgenic zebrafish embryos using BODIPY TR methyl ester dye as a vital counterstain for GFP. *Dev Dyn* 2005;232:359–68.